Hubble diagram and cosmology measurements

Martin Goliath, Dragan Huterer, and Eric V. Linder

Abstract

For rigorous estimation of cosmological parameters we demand three properties of any probe: 1) precise observations - measurements with small statistical errors, bountiful measurements, standardizable measurements with small, understood systematic errors, and measurements over a range in redshift; 2) accurate models - arising from simple, well determined physics, replete with cross checks, possessing cosmological leverage (not dependent on one redshift or on an intricate combination of cosmological parameters); 3) complementarity - combinable with other probes to cross check and break degeneracies. At the present state of our astrophysical understanding the Type Ia supernova Hubble diagram best fulfills all three of these conditions for the recent universe.

1 Hubble Diagram

The Hubble diagram, or magnitude-redshift relation, for supernovae transparently traces the expansion history of the universe. For calibrated candles such as Type Ia supernovae apparent magnitude represents luminosity distance or equivalently lookback time to the supernova explosion – dimmer means farther in the past. The redshift measures the expansion factor a since that time, so the magnitude-redshift diagram gives $a(t)$ directly. Curvature in the Hubble diagram probes evolution in the expansion rate – acceleration or deceleration – directly related to the values of the component energy densities, dark energy equation of state, and fate of the universe.

The magnitude or luminosity distance-redshift test probes differing combinations of cosmological parameters in different redshift ranges. This is one of its great strengths in that not only is it most sensitive to changes, e.g. acceleration, occurring in the expansion history of the universe at recent times, but it provides 1) complementarity to high redshift tests, other medium redshift tests, and even itself; 2) detection of evolution in the state and nature of the universe by probing different epochs than the cosmic microwave background, say, and different energy densities (smooth components) than large scale structure tests; 3) protection against secular or differently evolving systematic effects such as grey dust.

Figure 1 shows the Hubble diagram that combines 18 Calan-Tololo SNe Ia as well as 42 SNe obtained by the Supernova Cosmology Project, out to $z \approx 0.8$, while Figure 2 shows a Hubble diagram with about 2800 SNe out to $z = 1.7$, expected after one year of operation of the proposed Supernova/Acceleration Probe (SNAP) satellite. The large number of supernovae throughout the redshift range will enable accurate measurements of cosmological parameters (see Fig. 3), as well as checks on systematics such as supernova evolution.

2 Redshift Range Requirements

At small redshifts the comoving distance $r(z)$ is insensitive to the dark energy equation of state w for the simple reason that *all* cosmological models reduce to the Hubble law ($r = H_0^{-1} z$) for $z \ll 1$,

$$r(z) \approx H_0^{-1}\left[z - z^2\left(\frac{1}{2} + \frac{1}{4}(\Omega_M + \Omega_X) + \frac{3}{4}w\Omega_X\right) + \cdots\right] \quad \text{for } z \ll 1. \tag{1}$$

At medium redshifts, $z \approx 0.5-1$, the matter density overtakes the dark energy density in both magnitude, at $z_{\rm eq}$, and dynamical influence, at the transition from accelerated to decelerated expansion at $z_{\rm ac}$, as seen in Fig. 4.

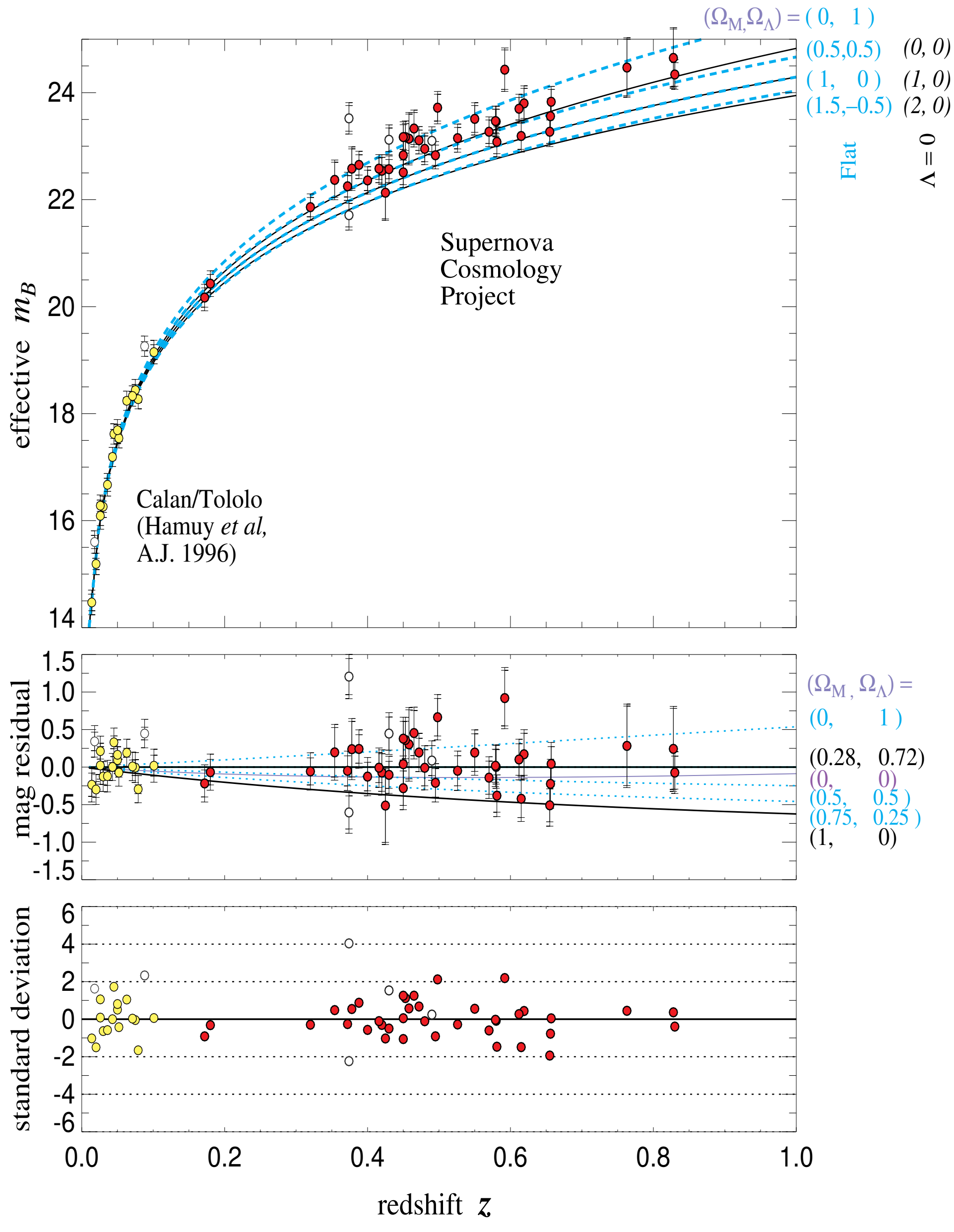

Perlmutter, *et al.* (1998)

Figure 1: Hubble diagram with 42 high-redshift supernovae with magnitude residuals from best fit cosmology.

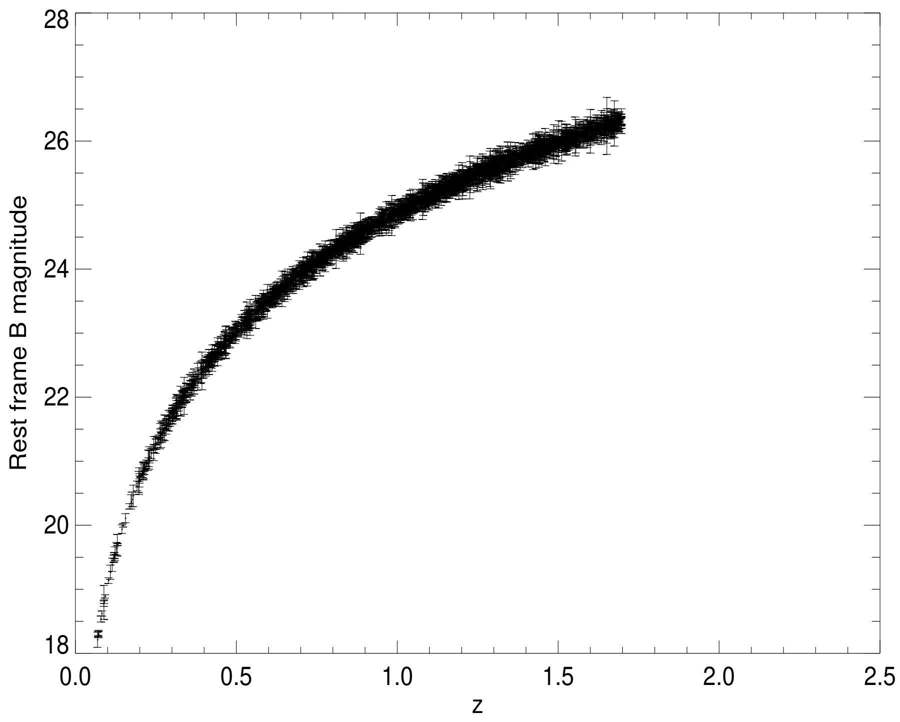

Figure 2: Hubble diagram with supernovae as expected from one year operation of SNAP.

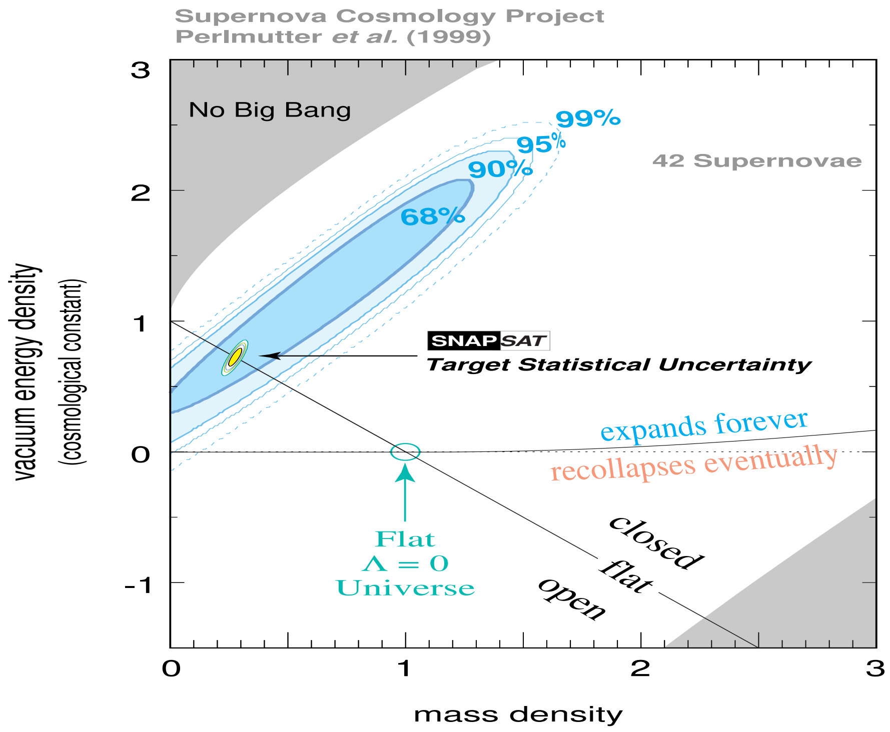

Figure 3: Confidence regions in the Ω_M-Ω_Λ plane from 42 high redshift SNe Ia in Perlmutter et al. (1999) and as expected from one year operation of SNAP.

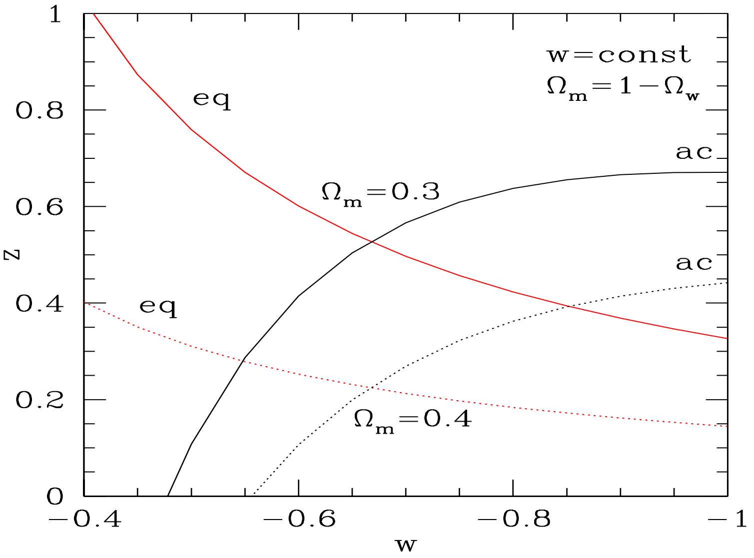

Figure 4: The redshifts of matter-dark energy equality and of the transition from decelerating to accelerating expansion are plotted vs. equation of state of the dark energy, for a flat universe. The solid curves have $\Omega_M = 0.3$, the dotted $\Omega_M = 0.4$.

At high redshift ($z \gtrsim 5$), the sensitivity of $r(z)$ to w levels off because dark energy becomes an increasingly smaller fraction of the total energy density, $\rho_X/\rho_M \propto (1+z)^{3w}$.

Figure 5 shows this, along with the sensitivity of other variables: the Hubble parameter $H(z)$ and the comoving volume element (differential comoving volume per unit redshift per unit solid angle), $f(z) \equiv dV/(dz\,d\omega) = r^2(z)/H(z)$, at the heart of number-redshift tests (e.g., counts of lensed quasars, galaxies, or clusters of galaxies).

Therefore, observations over the redshift range $0 \lesssim z \lesssim 2$ will be most useful in probing dark energy. Figure 6 makes this more quantitative, showing the accuracy of the determination of w (assumed constant) as a function of maximum redshift probed $z_{\rm max}$. For $0.2 \lesssim z_{\rm max} \lesssim 1$, the 1σ uncertainty σ_w decreases sharply and then levels, with little decrease for $z_{\rm max} \gtrsim 1.5$.

While the sensitivities in Fig. 5 peak at $z \approx 0.5-1$, as do the transitions in Fig. 4, this region is not the whole story. For one thing, higher redshift SNe are very important to help break parameter degeneracies. To illustrate the importance of having high redshift supernovae, we investigated the effect of adding 100 supernovae to a large initial sample at lower redshift: 2000 supernovae uniformly distributed in the interval $z \in [0.2, 1.2]$. Figure 7 shows the effect on the errors of Ω_m and Ω_X when adding 100 supernovae to the samples outlined above. As expected, high redshifts pay off when determining Ω_m and Ω_X, but in case the knowledge of $\mathcal{M}$ is poor, it is also important to fill in the low redshift region. In fact one can prove [2] that there are three "sweet spots" in redshift when Ω_M and Ω_X are to be determined: $z = 0$, $z = z_{\rm max}$, and $z \approx (2/5)z_{\rm max}$.

Second, to discriminate *between* dark energy models, whether between cosmological constant, constant w models, or evolving $w(z)$ quintessence models, it is necessary to extend the survey depth to $z \approx 1-2$. This reveals the physical imprint of differential acceleration, the dilution of the effective equation of state due to the increasing dominance of matter, and the turnover to a decelerating expansion including the "inertia" of the magnitude-distance relation that integrates over the equation of state from the source epoch to the present [3].

3 Statistical Uncertainties for Parameter Estimation

Data on supernovae peak magnitudes, with uncertainties, over a redshift range are translated into cosmological parameter estimation. We investigate the accuracy of these estimations based on one year of data

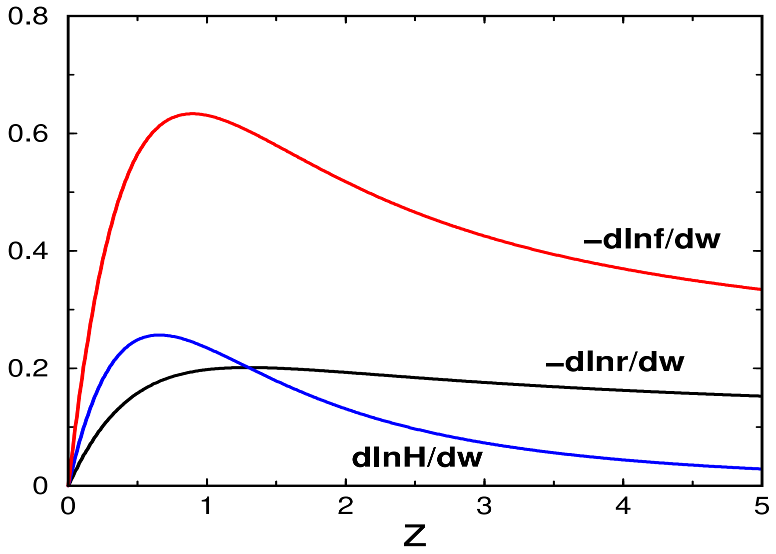

Figure 5: The relative sensitivity of $r(z)$, $f(z)$, and $H(z)$ to a change in the constant value of w.

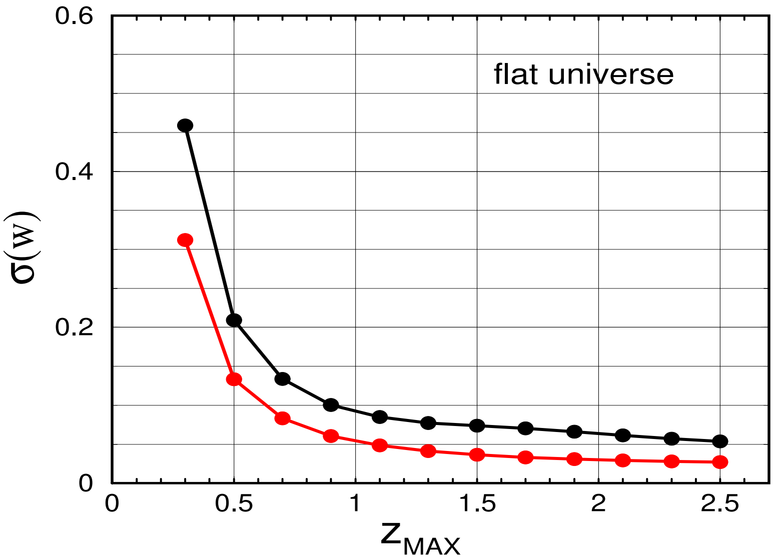

Figure 6: Estimated 1σ errors in determining (constant) w as a function of maximum redshift probed $z_{\max}$ for a flat Universe, 2566 SNe and marginalizing over the other parameter, Ω_M. The upper curve shows the uncertainties using the fiducial SNAP distribution cut-off at $z_{\max}$ and renormalizing to keep the total number of SNe constant. The lower curve shows uncertainties obtained using the mathematically optimal distribution, with equal number of SNe located at each of three redshifts: $z = 0$, $z \approx 2/5\, z_{\max}$ and $z = z_{\max}$.

in the SNAP scenario ([5]; an intrinsic peak magnitude dispersion of SNe Ia of 0.15 magnitudes with ~ 50 supernova per redshift bin gives a magnitude uncertainty of 0.02 magnitudes), and some variations on it (see [1] for more detail).

Effect of adding 100 SNe to initially 2000 uniformly in (0.2, 1.2)

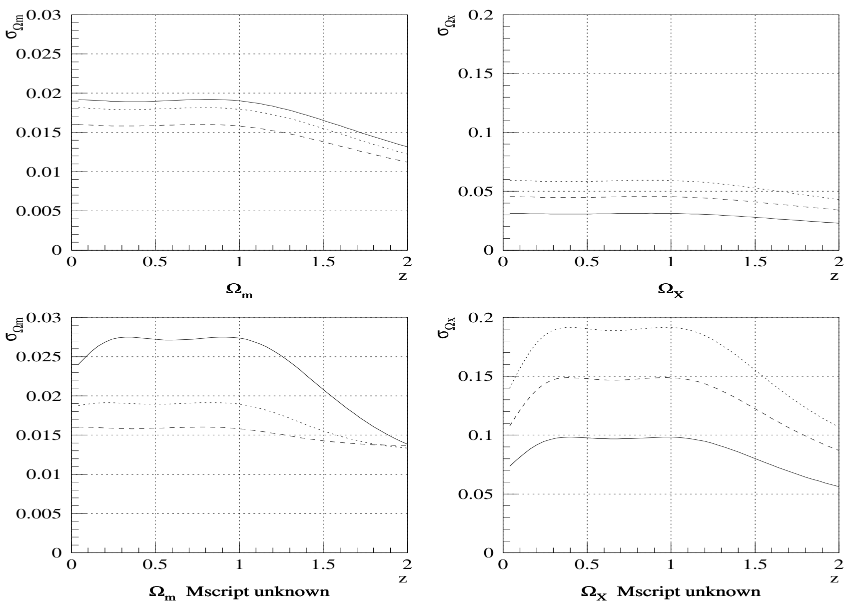

Figure 7: The effect on the uncertainties in Ω_M and Ω_X of adding 100 SNe at a given redshift, for three different $w(z)$. The top panels assume the supernova absolute magnitude $\mathcal{M}$ is known, the bottom unknown.

3.1 Confidence regions for $(\Omega_m, \Omega_\Lambda)$

First, let us assume that the dark energy corresponds to a cosmological constant $\Omega_X = \Omega_\Lambda$, i.e. $w = -1$. Figure 8 shows confidence regions for $(\Omega_m, \Omega_\Lambda)$ for various situations. We see:

- The few events at high redshift ($z > 1.2$) result in about 25 % better determination of Ω_Λ. This emphasizes the importance of obtaining at least a few supernovae at high redshift.
- Lack of prior knowledge of $\mathcal{M}$ (the supernova absolute magnitude folded with the Hubble constant) severely degrades the precision in Ω_Λ. This illustrates the importance of having supernovae at *low* redshifts.
- Prior knowledge of Ω_m with $\sigma_{\Omega_m-\text{prior}} = 0.05$ Gaussian around the true value is too rough to appreciably enhance the precision.

3.2 Confidence regions for (w_0, w_1)

Next, we allow for $w \neq -1$ and consider the ability to determine the equation of state of the dark energy to linear order, $w(z) = w_0 + w_1\, z$, assuming flatness and some prior knowledge of Ω_m. Figure 9 shows confidence regions for various situations. We find:

- When $\mathcal{M}$ is exactly known, the few high-z supernovae are not so important in determining (w_0, w_1) as they are for (Ω_m, Ω_X), basically because Ω_X becomes less significant with increasing redshift. However the high-z events make some difference when $\mathcal{M}$ is poorly known.
- The precision degrades considerably when there is no prior information of $\mathcal{M}$.

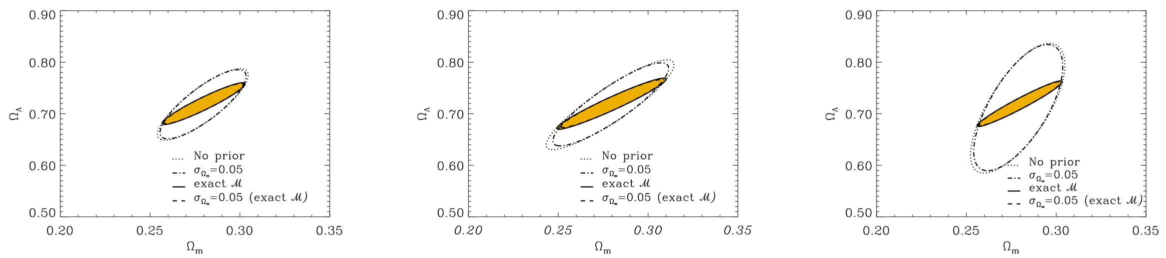

Figure 8: 68.3 % confidence regions for $(\Omega_m, \Omega_\Lambda)$. The first panel is for the one-year SNAP scenario; the middle one is for the one-year SNAP scenario without the 100 events at $z \in [1.2, 1.7]$; and the last panel is for the one-year SNAP scenario with a constant rate per co-moving volume for $z \in [0, 1.2]$, and the 100 $z \in [1.2, 1.7]$ events uniformly distributed. The filled region (solid line) assumes exact knowledge of $\mathcal{M}$, and the dashed line within the filled region assumes also a prior knowledge with Ω_m Gaussian around the true value and $\sigma_{\Omega_m-\mathrm{prior}} = 0.05$. A full three-parameter fit with no prior knowledge of $\mathcal{M}$ is assumed for the two larger confidence regions: the region with a dotted line assumes no prior knowledge of Ω_m, while the dash-dotted line assumes a prior knowledge with Ω_m Gaussian around the true value and $\sigma_{\Omega_m-\mathrm{prior}} = 0.05$.

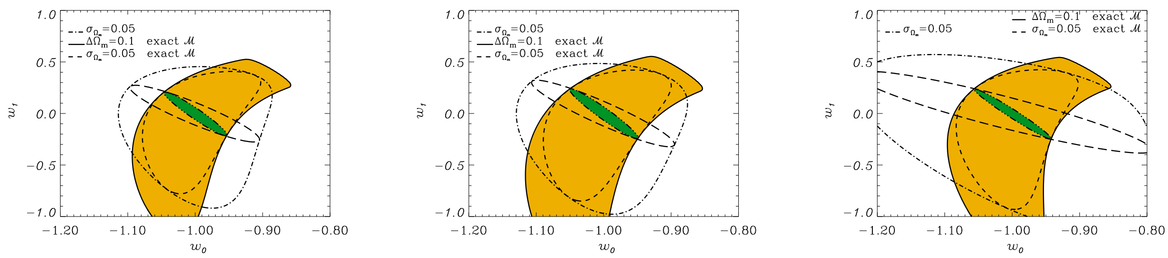

Figure 9: 68.3 % confidence regions for (w_0, w_1). The first panel is for the one-year SNAP scenario; the middle one is for the one-year SNAP scenario without the 100 events for which $z \in [1.2, 1.7]$; and the last panel is for the one-year SNAP scenario with a constant rate per co-moving volume for $z \in [0, 1.2]$, and the 100 $z \in [1.2, 1.7]$ events uniformly distributed. The elongated ellipses correspond to the assumption of exact knowledge of Ω_m: the dash-dot-dot-dotted line is with exact $\mathcal{M}$ and the long-dashed line corresponds to no knowledge of $\mathcal{M}$. The larger, non-elliptic regions assume prior knowledge of Ω_m: the dash-dotted line assumes that Ω_m is known with a Gaussian prior for which $\sigma_{\Omega_m-\mathrm{prior}} = 0.05$; the short-dashed line assumes the same prior and exact knowledge of $\mathcal{M}$; finally, the solid line is with Ω_m confined to the interval $\Omega_m \pm 0.1$ and exact knowledge of $\mathcal{M}$.

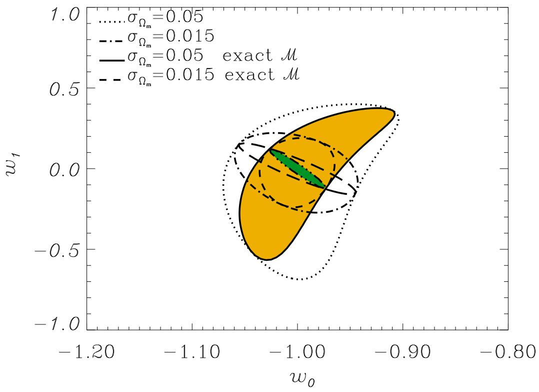

Figure 10: 68.3 % confidence regions for (w_0, w_1) in the three-year SNAP scenario. The elongated ellipses correspond to the assumption of exact knowledge of Ω_m: the dash-dot-dot-dotted line is with exact $\mathcal{M}$ and the long-dashed line corresponds to no knowledge of $\mathcal{M}$. The larger, non-elliptic regions assume Gaussian prior knowledge of Ω_m: the dotted line is with $\sigma_{\Omega_m-\text{prior}} = 0.05$, while the dash-dotted line is with $\sigma_{\Omega_m-\text{prior}} = 0.015$. The solid and short-dashed lines assume exact knowledge of $\mathcal{M}$ with the same Ω_m priors as above.

To better constrain the equation of state we consider the expected three years of SNAP operation (i.e. three times as many supernovae) and a sharper prior $\sigma_{\Omega_m-\text{prior}} = 0.015$, consistent with the estimated precision of a hypothetical ground based $10^\circ \times 10^\circ$ weak lensing survey ([6]; note SNAP will carry out a 300 square degree space based lensing survey). Uncertainties in w_0 and w_1 go down to $w_0 = -1 \pm 0.02$, $w_1 = 0^{+0.13}_{-0.15}$ with an exact $\mathcal{M}$, and $w_0 = -1 \pm 0.04$, $w_1 = 0^{+0.15}_{-0.17}$ with no prior on $\mathcal{M}$, constraining the nature of the dark energy quite well as seen in Fig. 10.

4 Discussion

It is important to realize that data at low as well as high redshift are required for optimal parameter estimation. Events at very low redshift help to fix the intercept $\mathcal{M}$, while a wide range of redshifts is needed to address systematics and to break the degeneracies in the luminosity distance between different cosmologies and different dark energy models. Complementary constraints, e.g. on Ω_M or Ω_{tot}, from other cosmological probes play a crucial role in limiting the parameter space of alternate models.

The expansion history of the universe revealed redshift by redshift by supernovae and other measurements sets forth the dark energy nature and evolution in a kind of cosmic tomography and directly probes the vacuum energy potential. With the Hubble diagram fulfilling the criteria listed in the introduction for a rigorous probe, we have the potential to advance as one our cosmological and fundamental physics understanding.

References

[1] Goliath, M., Amanullah, R., Astier, P., et al. (2001), preprint, astro-ph/0104009.

[2] Huterer, D. & Turner, M. S., *Phys. Rev. D*, in press (astro-ph/0012510)

[3] Linder, E.V. (2001), preprint, astro-ph/0108280.

[4] Perlmutter, S., Aldering, G., Goldhaber, G., et al. (1999), *Astrophys. J.* **517**, 565.

[5] Supernova / Acceleration Probe (SNAP) (2000), http://snap.lbl.gov/

[6] van Waerbeke, L., Bernardeau, F. & Mellier, Y. (1999), *Astron. Astrophys.* **342**, 15.